JORDAN JOURNAL OF BIOLOGICAL SCIENCES

Jordan Journal of Biological Sciences

Journal homepage: www.jjbsci.com

In Silico Evaluation of KIF1A Gene Variants Revealing Structural Destabilization and ATP-Binding Alterations in KAND

Bharati Sidambaram [1], Sakshara Shetty [1], Annliya Biju [1], Deekshitha M [2*]

[1] Department of Biotechnology, M S Ramaiah Institute of Technology Bengaluru, Karnataka, India-560054.
[2] Department of Bioinformatics, BioNome, Bengaluru, Karnataka, India-560043.

To cite this article: Bharati Sidambaram, Sakshara Shetty, Annliya Biju, Deekshitha M(2026) In Silico Evaluation of KIF1A Gene Variants Revealing Structural Destabilization and ATP-Binding Alterations in KAND; JJBS; 18:1, 9:24.

Corresponding author:

Deekshitha M

Department of Bioinformatics, BioNome, Bengaluru, Karnataka, India-560043

Email: info@bionome.in

ORCID:

Bharati Sidambaram: https://orcid.org/0009-0006-4782-587X

Sakshara Shetty: https://orcid.org/0009-0007-3853-9326

Annliya Biju: https://orcid.org/0009-0006-2633-5820

Deekshitha M: https://orcid.org/0009-0008-0437-7266

ABSTRACT

KIF1A associated neurological disorder (KAND) is an umbrella of neurological disorders caused by mutations in the *KIF1A* gene. These mutations lead to various neurological disorders such as hereditary spastic paraplegia, sensory neuropathy, intellectual disability, and progressive encephalopathy. This project is aimed to isolate and differentiate nsSNP (Non- Synonymous Single Nucleotide Polymorphism) based on deleteriousness, disease causal or pathogenicity, effect on stability, evolutionary conservation and functional impact. To further validate the findings, tertiary structure modelling, docking, and dynamic studies were carried out. The variants were collected from 2 databases: dbSNP and ClinVar, which were then screened and the common mutations were retrieved for further analysis. Deleterious effect was predicted by tools such as SIFT, AlignGVGD, and dbNSFP. The mutations were then classified based on disease-causing and neutral effects through various tools like SNP & GO, PhD-SNP AND META-SNP. The degree of conservation of amino acid residues of the sequence was assessed using the ConSurf tool. This helps understand the evolutionary conservation, indicating the impact on protein structure and function by the residue. This was followed by functional impact prediction by MutPred to show the various changes brought about by nsSNPs on the overall function of the protein. Molecular docking by AutoDock Vina analyses the binding affinity of ATP with wild-type protein and the mutated protein. The stability simulated in real-world conditions over a period of time is predicted using Molecular Dynamics by GROMACS that evaluates the RMSF, RMSD, H-bond, Rg, SASA, PCA and FEL analysis of the two protein structures. This multi-step pipeline concludes with nsSNPs with the most potential to cause the disease, and be used as a potential drug target for treating KAND.

Keywords: *KIF1A; nsSNPS; Mutations; R350G; Insilico; KAND*

ARTICLE HISTORY

Received 05 Jan 2026
Accepted 22 Jan 2026

INTRODUCTION

Kinesin acts as a catalyst in the hydrolysis of adenosine triphosphate (ATP), facilitating the conversion of chemical energy into mechanical energy that drives the movement of microtubules and the transport of organelles and intracellular components. The KIF family of proteins constitutes a subset of kinesins. Among them, kinesin family member 1A (KIF1A) belongs to the kinesin-3 family, typically existing in a monomeric form and functioning as a plus-end-directed motor protein along microtubules [1]. KIF1A encodes a kinesin-3 motor protein responsible for transporting synaptic vesicle precursors, dense-core vesicles, active zone precursors, and other essential cargoes along neuronal microtubules over long distances [2, 3]. Structurally, KIF1A contains three major domains: the head, stalk, and tail domains. The head domain is responsible for motor activity, the stalk domain enables dimerization, and the tail domain mediates cargo binding [4]. KIF1A transports critical post-synaptic cargoes such as GRIP, GIT1, AMPA receptors, and the neurotrophin receptor TRKA, which are essential for neuronal development, synaptic plasticity, and survival. Cargo binding promotes KIF1A dimerization, thereby enhancing its processivity [3]. Synaptic vesicle transport is fundamental to synapse formation and function, and targeted delivery to axonal regions contributes to axon identity and neuronal polarity. Moreover, KIF1A plays an essential role in neurite outgrowth and synaptic maturation, processes crucial for brain development and cognitive function [5].

Functionally, KIF1A primarily transports synaptic vesicle precursors (SVPs) containing proteins such as synaptophysin, synaptotagmin, and the small GTPase RAB3A, but it does not transport plasma membrane proteins. Through the adaptor protein DENN/MADD, KIF1A binds to RAB3-carrying vesicles, recognizing RAB3 exclusively in its GTP-bound state to ensure that only active vesicles are transported. While the PH domain aids in lipid binding, the interaction between RAB3 and DENN/MADD is critical for the transport process [6]. Given the crucial role of KIF1A in neuronal function, its proper operation is essential for maintaining synaptic activity, axonal transport, and neuron survival. Mutations in KIF1A lead to a group of rare neurological and motor disorders collectively termed KIF1A-associated neurological disorders (KAND) [2]. These disorders manifest as intellectual disability (ID), spasticity, and axial hypotonia, often accompanied by optic atrophy, growth failure, and progressive cerebellar atrophy, which are commonly linked to de novo KIF1A mutations [7]. Several conditions have been associated with KIF1A mutations. Hereditary spastic paraplegia (HSP) arises from mutations that impair SVP transport and result in synaptic dysfunction. Hereditary sensory and autonomic neuropathy type IIC is associated with recessive mutations that disrupt axonal transport in sensory neurons. Intellectual disability and developmental delay stem from defective trafficking of synaptic and signaling vesicles, leading to disturbances in cortical development and synaptic plasticity [5].

Genetic variations in humans are largely represented by single nucleotide polymorphisms (SNPs), which account for phenotypic diversity among individuals. Non-synonymous SNPs (nsSNPs) occur in the coding regions of genes, leading to amino acid substitutions that may alter protein structure or function [8]. These nsSNPs have been implicated in a wide range of diseases, as many occur within or near protein

interaction interfaces. Such alterations can disrupt normal protein–protein interactions, weakening binding affinities or converting transient complexes into stable ones. Disruptions in these networks often result in cellular misregulation, contributing to diseases such as cancer, diabetes, and immune disorders [9]. However, not all nsSNPs are deleterious—some are neutral and exert minimal or no impact on protein stability or function. Therefore, it is essential to employ computational tools and empirical criteria to distinguish deleterious nsSNPs from neutral variants [9,10]. Identifying deleterious functional nsSNPs is vital for understanding the molecular basis of disease. However, assessing a single nsSNP is often insufficient to capture the complexity of protein alterations and drug responses. To overcome this, in silico methods have been developed to analyze groups of nsSNPs across the genome, enabling the identification of variants that influence protein interactions, drug targets, and metabolic enzymes [11]. These approaches enhance the understanding of genotype–phenotype relationships and aid in predicting individual drug responses.

In this study, variant interpretation was performed using ClinVar and dbNSFP databases. By comparing nsSNPs and classifying them as deleterious or neutral polymorphisms, this work establishes a foundation for subsequent modeling and functional interpretation [12]. Furthermore, structural analysis and binding affinity evaluations through molecular docking revealed altered protein function, with mutant KIF1A exhibiting higher ATP-binding affinity than the wild type. These findings highlight key regulatory regions influencing axonal transport, microtubule motor activity, and synaptic transmission. Mutations appear to weaken inhibitory interactions between the stalk and motor domains, resulting in enhanced microtubule binding by the mutant protein [13]. Finally, molecular dynamics simulations provided insights into the structural and functional consequences of specific amino acid substitutions. The analyses revealed alterations in energy interactions that compromise motor performance, structural integrity, and folding characteristics. Moreover, the simulations captured dynamic parameters such as atomic fluctuations, hydrogen bonding, solvent accessibility, and electrostatic interactions that collectively define the conformational behavior of the mutant protein [14].

METHODYLOGY

2.1. Retrieval and Compilation of KIF1A nsSNPs

Retrieval of nsSNPs were obtained from dbSNP (https://www.ncbi.nlm.nih.gov/snp) and Clinvar (https://www.ncbi.nlm.nih.gov/clinvar) to provide comprehensive information on genetic variation and evaluation. dbSNP was used due to its largest public source single nucleotide polymorphism which validates identifiers and allele frequency [15]. Clinvar captures suspected variants with clinical significance that allows to relate nsSNP with disease phenotypes [16].

In this project, the gene name KIF1A of *Homo sapiens* were given in the search to ensure that only human gene specific variants were retrieved. Clinvar links sequences with variation to phenotypic outcomes and classifies based on pathogenicity whereas dbSNP is a central archive providing functional classification and frequency data of genetic variation.

2.2. Prediction of Functionally Deleterious nsSNPs

SIFT (https://sift.bii.a-star.edu.sg/) was used to classify and predict whether the amino acid substitution by nsSNP will affect protein function (tolerated or intolerated). It uses sequence homology and conservation of amino acid residues to classify. Scores usually range between 0 to 1, whereas scores below 0.05 indicate damaging substitutions. The 1198 common rsIDs were given as input to the SIFT tool [17]. These were classified based on tolerated (score > 0.05) and deleterious (score < 0.05) [18].

dbNSFP database (https://www.dbnsfp.org/) was used to predict whether the nsSNP was deleterious or neutral. The tools used were Provean, Vest4, MetaLR and REVEL . The rsIDs of the 25 SNPs were given as input. Multiple algorithms were used to improve reliability and accuracy. In all these tools, predictions are given as a probability score ranging from 0 to 1, with scores >0.5 indicating a disease-causing effect and scores ≤0.5 considered neutral. These probabilities are derived from ML models that integrate sequence, evolutionary, and functional features to estimate the likelihood that a given variant impacts protein function and contributes to disease [19].

Align GVGD (https://agvgd.hci.utah.edu/) is used to predict whether nsSNPs were deleterious or neutral based on the evolutionary conservation and characterisation of amino acids. It measures the evolutionary variation with the protein position by combining Grantham Variation (GV) and Grantham deviation (GD) which measures between wild- type and mutant amino acids. The FASTA sequence of proteins, along with the substitution list of the 6 mutations identified by SIFT as well as screened by dbNSFP were used as input. Align-GVGD classified these and predicted variants as Class 65, which is the most deleterious category strongly associated with disease-causing potential, and the intermediate classes (Class 25–45), which are less likely disease-causing [20].

2.3. Identification of Disease Associated nsSNPs

The input consisted of amino acid substitution retrieved from FASTA and gene ontology terms from the UniProt database of 5 mutations having deleterious effects. SNP&GO (https://snps-andgo.biocomp.unibo.it/snps-and-go/) was used to improve reliability in predicting functional annotations by Gene Oncology (GO) terms. The usual probability score is from 0-1 [18]. The scores greater than 0.5 is disease causing and less than 0.5 is considered neutral.

PHD SNP (http://snps.biofold.org/phd-snpg) was used to classify nsSNP as a disease causing or neutral using an SVM based model. The FASTA sequence of the full wild-type protein from UniProt, position of each mutation, and new residue in each mutation given as input and sequence-based prediction was done. Phd-SNP incorporates evolutionary conservation and sequence features to predict the effect of variants. If the score is above 0.5 it is considered disease

causing and less than 0.5 is considered neutral [21].
META SNP (http://snps.biofold.org/meta-snp/) was used to obtain high prediction accuracy by combination of multiple algorithms. In this, FASTA sequence of the wild type, and 3 mutations that are disease-causing are retrieved from FASTA and given as input. The incorporation of Machine learning prediction, reducing the bias and increasing accuracy. The scores greater than 0.5 is disease causing and less than 0.5 is considered neutral.

2.4. Evaluation of Protein Stability Effects

3 deleterious and disease-causing SNPs obtained from Meta-SNP were given as input to 2 stability predicting tools. MuPro (http://mupro.proteomics.ics.uci.edu/) and DUET (http://bleoberis.bioc.cam.ac.uk/duet/) are tools to measure the change in Gibb's free energy. Negative ΔΔG (< 0) represents decrease in protein stability, or destabilizing effect, and positive ΔΔG (> 0) indicates increase in stability, which is a stabilizing effect [22, 23].
Amino acid residues in the wild type, its mutation, and FASTA sequence of the protein were given as input to MuPro. For DUET, the structure was modelled using SWISS-MODEL and given as input. Both the models provide information on mutations that compromise protein stability [23].

2.5. Evolutionary Conservation Analysis

ConSurf (http://consurf.tau.ac.il) analysis was carried out to evaluate the evolutionary conservation of SNPs. The tool assigns a conservation score ranging from 1 (highly variable) to 9 (highly conserved). In this analysis, the FASTA sequence of the wild type KIF1A protein was given as input. Residues with a score close to 9 are evolutionarily conserved across multiple species, suggesting that they play a crucial role in maintaining the structural stability or functional activity of the protein. Mutations occurring at these highly conserved sites are therefore more likely to disrupt protein function and contribute to disease [24].
ConSurf also classifies residues as either functional (f), when they are exposed and conserved, or structural (s), when they are buried and conserved, which affect the functioning and 3d structure folding respectively.

2.6. Tertiary structure modelling and Validation

The homology model of the wild type protein was generated using Swiss-Model (http://swissmodel.expasy.org/repository/) by giving its FASTA sequence, selecting a template with sequence identity and Global Model Quality Estimation (GMQE) greater than 0.6, indicating a reliable model [25]. The 2 nsSNPs showing highly deleterious, disease associated, decreasing protein stability had most promising mutations in the KIF1A gene, for which the tertiary structure was modelled using Pymol, followed by Swiss-Model. The wild-type protein structure was subjected to site-directed mutagenesis using the Mutation Wizard tool, where specific amino acid substitutions were introduced. The resulting mutant structures were saved in PDB format.
The Ramachandran plot (https://saves.mbi.ucla.edu/) classifies residues based on their backbone torsion angles (φ and ψ) into regions that reflect the quality of protein folding. The input for obtaining the plot and the ERRAT score was the pdb files of the wild type and the 2 mutations. The most favoured regions represent energetically stable and sterically favourable conformations, while the additionally allowed regions correspond to less favourable but still acceptable conformations. Generously allowed regions are rarely occupied conformations that can occasionally occur in flexible proteins, whereas disallowed regions correspond to sterically impossible conformations that usually indicate modelling errors or strained geometry [26].
The ERRAT score further validated the quality of the models by evaluating non-bonded atomic interactions and comparing them with high-resolution crystallographic data. Scores greater than 90 are considered great [27].

2.7. Prediction of Functional Impact of nsSNPs

MutPred (http://mutpred.mutdb.org/) provides probability predictions of the functional impact of amino acid substitutions, where higher scores (close to 1) indicate a greater chance of pathogenicity. In addition to that, MutPred also suggests specific molecular alterations such as disruption of ATP binding sites, allosteric sites, DNA binding, catalytic activity, post-translational modifications, or changes in structural features like helices and strands.
In this analysis, the amino acid sequence of the wild-type protein and amino acid substitution of the 2 destabilizing, highly conserved mutations which were known to affect structure and function were given as input. The high scoring mutations were analyzed and interpreted [28].

2.8. Protein- Ligand docking

Molecular Docking was conducted using AutodockVina (https://vina.scripps.edu/wp-content/uploads/sites/55/2020/12/autodock_vina_1_1_2_win32.msi) where the mutated protein and wild type were assessed individually. Molecular Docking expresses the structure and functional activity of nsSNP. It also gives insight on the conformational change and stability of the complex. The docking results were quantified based on their binding affinity that represents the energy associated with binding of KIF1A protein and ATP. The protein is prepared by removing water molecules, adding polar hydrogen and Kolman charge to it. The docked molecule has a Grid Box generated in the active site. On AutoDock tools, active site residues previously obtained were highlighted and appropriately placed in the Grid Box according to said residues to define the binding site. These results were visualised using PyMol. The docking scores were compared and Gibbs free energy (G in kCal/mol) was evaluated [29].

2.9. Molecular dynamics Simulations

The Molecular Dynamics Simulation (MDS) using GROMACS software was used to evaluate the stability of the R350G, and wild-type models. MDS was conducted using the GROMACS package with the CHARMM27 force field. Solvation was obtained using the SPC216gro water model, and a salt

concentration of 0.15 M with Na^+ and Cl^- ions was maintained, and the complex's pH was set at 7. The equilibration process consisted of two phases: first, a 20-ps v-rescale algorithm heating period gradually increased the temperature to approximately 310 K in the NVT ensemble. Then, a 20-ps restrained phase to allow solvent settling, followed by a 20-ps NPT equilibration phase with gradually removed restraints. Once equilibrated, the systems underwent a 100 ns preparation period for graphing and analysis, with pressure maintained at 1 atm and temperature at 310 K.

MDS assessed variations in Root Mean Square Deviation (RMSD), Root Mean Square Fluctuation (RMSF), Radius of Gyration (Rg), Solvent Accessible Surface Area (SASA), Principal component analysis (PCA), Free energy landscape (FEL), and hydrogen bond count of the complex, providing a comprehensive evaluation of its stability [30].

RESULTS

3.1. Retrieval of nsSNPs

Out of the total 54,030 SNPs retrieved from dbSNP, 2,128 were identified as non-synonymous SNPs. In the case of ClinVar, 3,373 SNPs were reported, of which 1,360 were nsSNPs after providing both tools an input of the gene and organism name (*KIF1A*, *Homo sapiens*). When comparing both datasets, an overlap of 1,198 nsSNPs that were common to both dbSNP and ClinVar were found. These overlapping variants are particularly valuable because they are supported by evidence from two independent databases, increasing their reliability. Hence, this common set of 1,198 nsSNPs was chosen for downstream analysis to ensure higher confidence in the results.

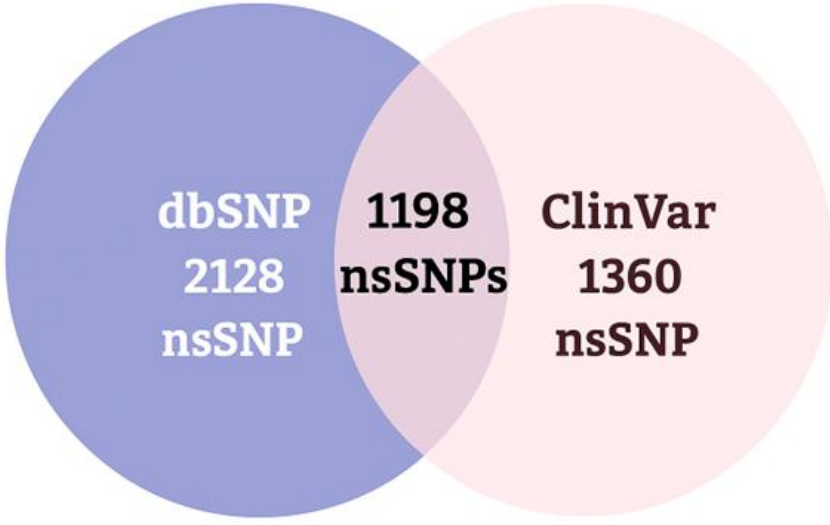

Figure 1: *Retrieval of nsSNP from dbSNP and ClinVar*

3.2. Prediction of Deleterious nsSNPs

A total of 1,198 common rsIDs were submitted to the SIFT tool predicting if amino acid substitutions are tolerated or deleterious based on sequence homology and conservation. From these, 938 returned as "Not Found" proving that the majority of SNPs . Predictions were available only for the remaining 260 SNPs. From these predictions, 235 were classified as tolerated (score > 0.05), while 25 were predicted to be deleterious (score < 0.05). Since deleterious variants are likely to disrupt protein function, these 25 SNPs were selected for further analysis using additional tools to predict and validate their deleterious and damaging effects.

Align GVGD and dbNSFP

As illustrated in Figure 3, the deleterious effect analysis was performed using both the standalone tool Align-GVGD and dbNSFP, which integrates multiple functional annotation tools.From dbNSFP, additional tools were screened. PROVEAN classified variants with scores ≤ –2.5 as deleterious, identified 22 variants as deleterious and 3 as tolerated. VEST4 predicted 15 deleterious and 8 non-deleterious variants. Similarly, MetaLR predicted 11 deleterious and 3 non-deleterious. REVEL (with scores ≥ 0.5 generally interpreted as deleterious), identified 6 deleterious and 5 non-deleterious. All 25 mutations identified were initially used as input. Align-GVGD further classified these, predicting 5 variants as Class 65, which represents the most deleterious category strongly associated with disease-causing potential.

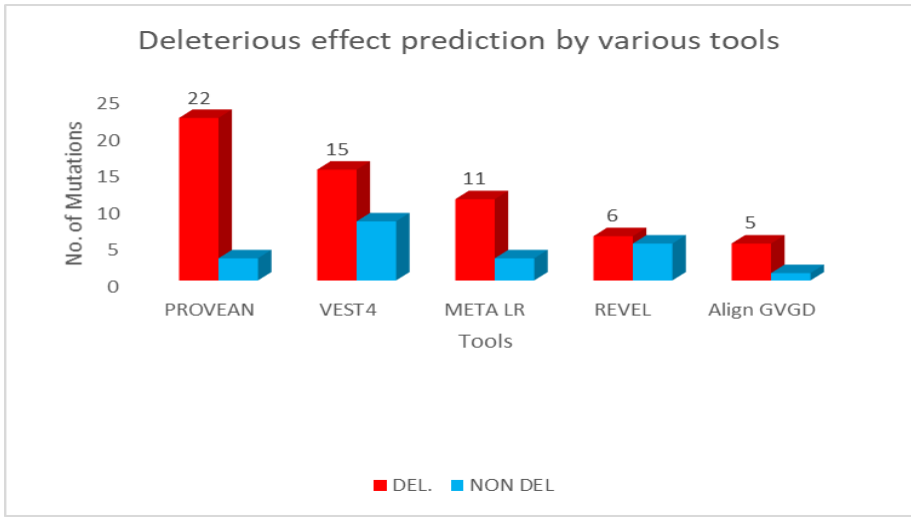

Figure 2: *Deleterious effect prediction by using Align GVGD and dbNSFP*

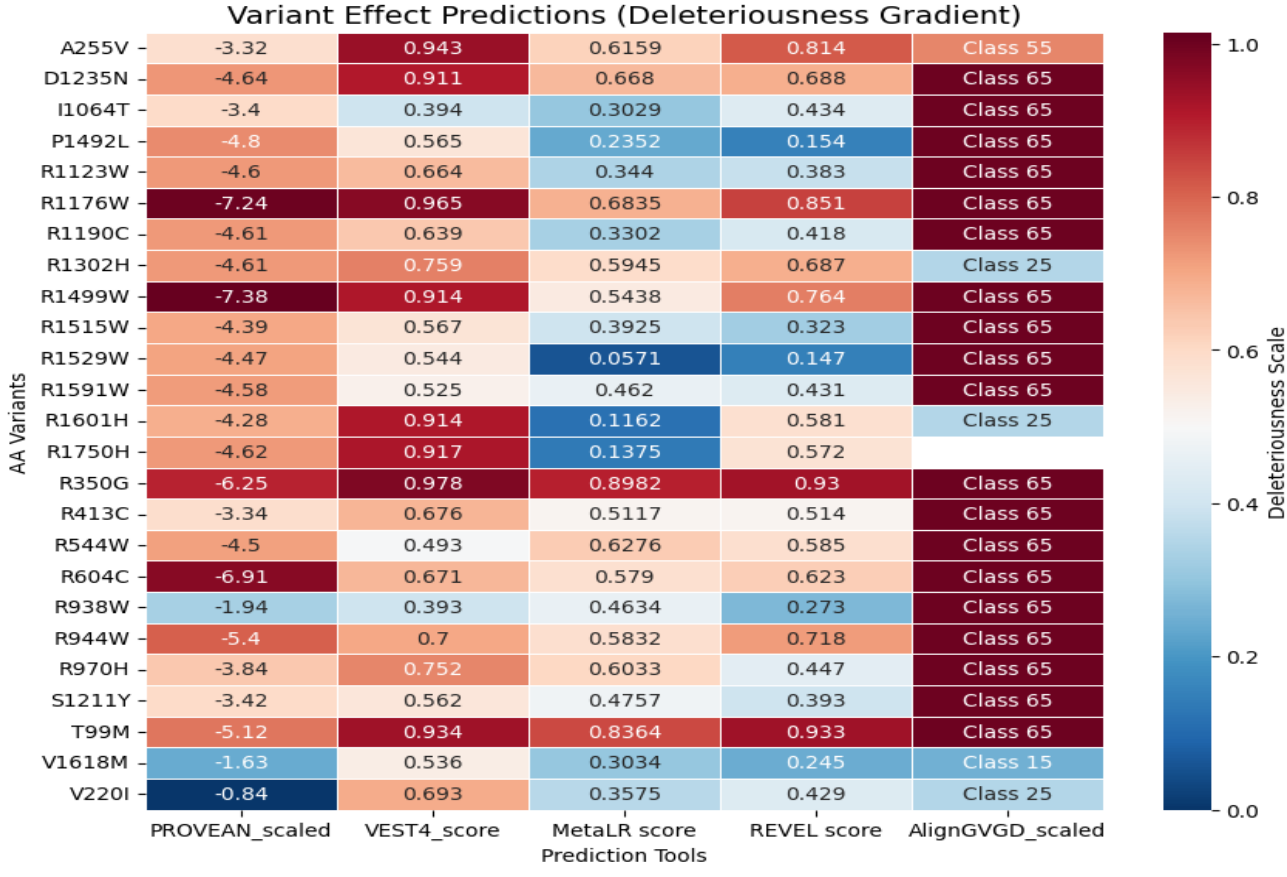

Figure 3: *Representation of overall scores and functional effects of nsSNP in KIF1A*

3.3. Disease Association Analysis of nsSNPs

From the 23 mutations analyzed in **Table 1**, Meta SNP predicted all 5 mutations as disease-causing and PhD-SNP predicted 4 disease-causing SNPs and 1 neutral. Similarly, SNP and GO predicted 3(R1176W, R350G, T99M) disease-causing and 2 (R1499W, R944W) neutral. This improvement reflects all the tools integrated and up-to-date algorithm, which combines multiple predictors to reduce false negatives and increase confidence in variant identification.

Table 1: *Various tools used for disease association analysis of nsSNP*

Mutation	META SNP		Phd SNP		SNP&GO	
R1176W	D	0.728	D	5	D	0.876
R1499W	D	0.735	D	4	N	0.166
R350G	D	0.901	D	4	D	0.807
R944W	D	0.663	N	0	N	0.44
T99M	D	0.901	D	4	D	0.829

3.4. Prediction based on Protein Stability effect

As shown in **Table 2**, out of the 3 SNPs evaluated, 2 mutations exhibited a destabilizing effect in both prediction tools, while only 1 mutation was consistently predicted to be stabilizing across both tools. DUET further provided structural insights by indicating that these destabilizing mutations predominantly occur within or affect loops and irregular secondary structure regions of the protein, which are often more flexible and functionally sensitive.

Table 2: *Stability-based prediction of nsSNPs by MuPro and DUET-based tool*

rs IDs	Mutation	MuPro		DUET based tool	
		ΔΔG (kcal/mol)	Prediction	ΔΔG (kcal/mol)	Prediction
rs374076405	R1176W	-1.2659051	Decrease	-0.349	Destabilizing
rs387907259	R350G	-1.1565879	Decrease	-2.013	Destabilizing
rs387906799	T99M	0.4476	Increase	0.431	Stabilizing

3.5. Evolutionary Conservation Analysis

Table 3 shows the 2 destabilizing mutations predicted based on protein stability effect taken for consurf analysis. Both of them were highly conserved with a score of 9. They are of type 'f' indicating that they are not only highly conserved but also present in the exposed region of the protein and thereby have an effect on the functioning of the protein and other molecular interactions.

Table 3: *Evolutionary Conservation-based analysis*

rs IDs	Mutation	Score	Type
rs374076405	R1176W	9	Highly conserved and exposed
rs387907259	R350G	9	Highly conserved and exposed

Figure 4: *Consurf results of amino acid residues of the protein. (a) 1-400 residues (b) 851 to 1200 Residues*

3.6. Tertiary structure modelling and Validation

The tertiary structure of the *KIF1A* wild was predicted using the SWISS-MODEL homology modeling server. The sequence was aligned with suitable templates to generate a reliable three-dimensional structure. Among the identified templates, F1M4A4.1.A was selected as the best template for modeling, exhibiting a high sequence identity of 97.63% and a GMQE score of 0.70, indicating a reliable structural prediction.

Table 5 shows that for both the wild type and all mutant structures, 85.2% of residues fell in the most favored regions, and 2.6% in disallowed regions. Additionally allowed and generally allowed regions varied among all 3 with a difference of 0.1% in each, but averaging around 10.2% and 2% respectively. These values are well within the acceptable range for reliable protein models, demonstrating that all the structures maintained good stereo chemical quality. The wild type and mutant proteins consistently showed ERRAT scores between 93.8 and 94.4, which further validates good quality of modelled structure. Figure 5 shows the tertiary structure visualization of the mutants, obtained through Biovia Discovery Studio. Figure 7 shows the Ramachandran plot of wild-type structure. An RC Plot has Φ (Phi) angle on the X-axis and Ψ (Psi) Y-axis which represent the backbone dihedral angles of amino acid residues.

The coloured regions represent show sterically allowed conformations where red indicates most favoured regions, bright yellow indicates additionally allowed regions, pale yellow indicates generously allowed regions and white represents disallowed regions. It was observed that majority of the residues lie in allowed regions, specifically in the right-handed alpha helix region, followed by beta sheet regions. Few residues outside the allowed regions indicate proline and glycine residues.

Table 5: *Distribution of amino acids in various regions given by RC Plot*

Protein	ERRAT scores	Ramachandran plot			
		Most favoured regions	Additionally allowed regions	Generously allowed regions	Disallowed regions
Wild type	93.8836	85.2	10.3	1.9	2.6
R1176W	94.3047	85.2	10.2	2	2.6
R350G	93.9439	85.2	10.1	2.1	2.6

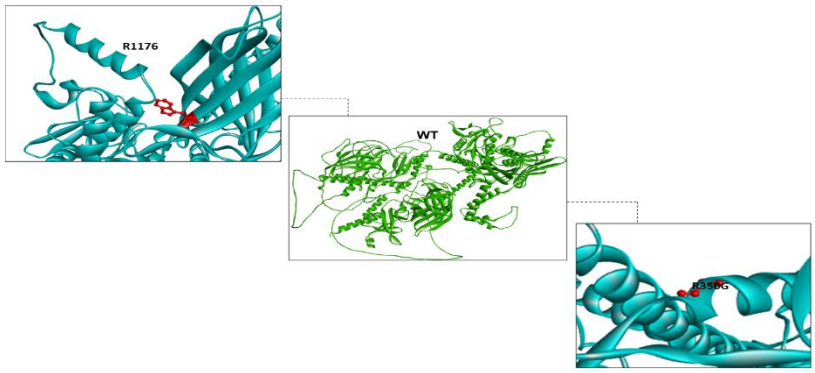

Figure 5: *Tertiary structure Visualization for the KIF1A wild and mutants (R1176, R350G)*

3.7. Based on Functional Impact

Out of 2 destabilizing mutations given as input, R1176W showed a score of 0.898 and R350G showed a score of 0.932, both of which indicate a high score and increased chances of pathogenicity and ability to alter function of the protein. **Table 6** explains the scores and the prediction of the associated mutations. R1176W is only predicted to alter the regulatory site of the protein. R350G is predicted to cause loss of secondary structure helix, and alters both ordered and disordered interfaces indicating that it affects the protein's interactions. It also alters the transmembrane protein which impacts signalling. It alters DNA binding which impacts regulatory activities and causes gain of methylation, which is introduction of a post-translational modification, which can alter protein stability and interactions further.

Table 6: *MutPred analysis of high-scoring mutations*

Mutation	Score	Prediction
R1176W	0.898	Loss of Allosteric site at R1175
R350G	0.932	Altered Disordered interface Loss of Helix Altered Ordered interface Altered Transmembrane protein Altered DNA binding Gain of Methylation at K352

3.8. Molecular Docking

Molecular docking analysis was done to compare the binding affinities of the wild-type *KIF1A* protein and its R350G mutant. The wild-type protein showed a binding affinity of –8.5 kcal/mol, whereas the R350G mutant showed a slightly higher affinity of –8.7 kcal/mol. Even though the difference in binding energies is small, the data implies that the R350G mutation may improve ligand binding relative to the wild type. The close similarity in docking scores shows that the mutation does not drastically change the overall binding surface as shown in **Figure 6**. But the observed increase in affinity in the R350G mutant could give insights on subtle conformational changes that impact ligand interaction dynamics.

Table 7: *Binding Affinity (kcal/mol) of Wild Type and R350G Mutant Type*

Protein	Binding Affinity (kcal/mol)
Wild Type	-8.5
R350G	-8.7

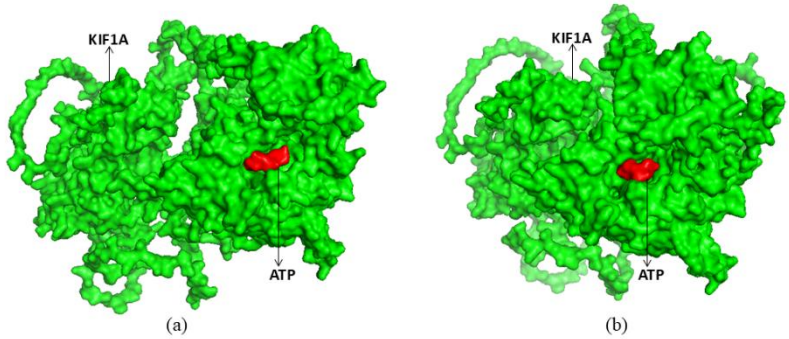

Figure 6: *Docking visualization for: a) wild type, b) mutant*

3.9. Protein-Ligand visualisation

The two-dimensional LigPlot+ representations (Figure 7) shows the important non-covalent interactions between ATP and the active-site residues of wild-type (WT) and R350G mutant (MT) KIF1A motor domains. In the WT–ATP complex, ATP forms many hydrogen bonds with residues Gly100(A), Gly102(A), Ala101(A), Lys103(A), Ser104(A), Tyr105(A), Asn200(A), Asn211(A), and Thr213(A), with bond lengths ranging between 2.59 Å and 3.27 Å. Three main hydrophobic residues- Thr99(A), Gly109(A), and Lys201(A) help in stabilizing the nucleotide via van der Waals and hydrophobic contacts indicated by residues circled in red in Figure 7(a). In the R350G mutant–ATP complex, the main hydrogen-bonding network remains conserved but additional bonds were seen with Ser214(A) and Arg203(A), along with changed bond geometries involving Asn200(A), Gly100(A), and Thr213(A). The mutant complex also displays new hydrophobic contacts with Lys110(A) and Met109(A), which replace the WT-specific hydrophobic regions near Thr99(A) and Lys201(A) as shown in Figure 7(b). These results remain consistent with the R350G mutant showing a slightly lower docking energy (–8.7 kcal/mol) compared to the WT (–8.5 kcal/mol), indicating a marginally higher binding affinity for ATP.

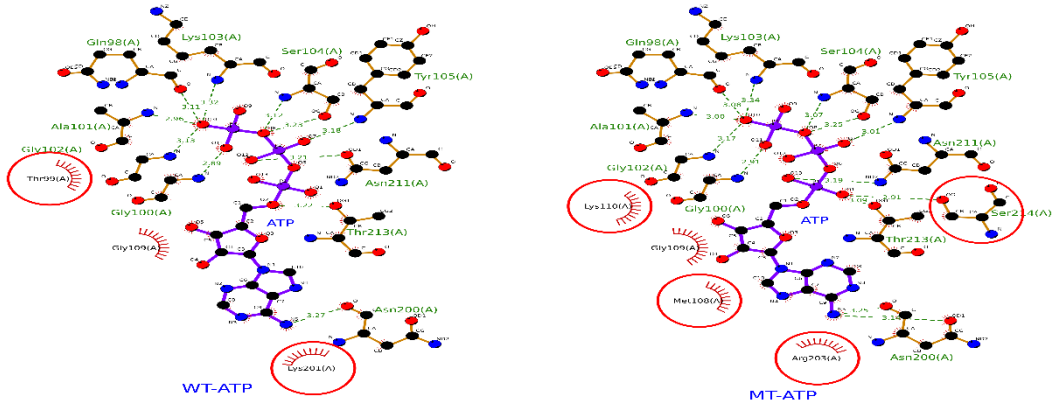

a) b)

Figure 7: *LigPlot visualization for: a) WT-ATP complex, and b) MT-ATP complex*

3.10. Molecular Dynamics Simulations

The RMSD graphs in (Figure 8(1)) shows the equilibrium was reached at 10-20 ns for both the wild type and the mutant type. After equilibration the mutant exhibited a steady high RMSD trace compared to the wild type, indicating structural rigidity loss. The RMSD fluctuations of Mutant type were also slightly larger, suggesting increased conformational change. The wild type and mutant type showed identical flexibility before RMSF which proved that most of the residues have similar flexibility but many localized regions showed clear differences. The Mutant type displayed increased flexibility at specific residue stretches as given in (Figure 8(2)) compared to Wild type, while other regions revealed comparatively reduced fluctuations. These changes localized to surface loop regions rather than the most rigid core secondary structure elements.

Time series of hydrogen-bonds (Figure 8(4)) showed that the mutant-type has a slightly lesser number of hydrogen bonds compared to wild-type across the trajectory, with higher short-term variability. The decrease is moderate and fluctuating, indicating the R350G substitution disturbs local hydrogen-bond networks without causing complete loss of secondary structure. Radius of gyration (Figure 8(3)) suggested that both systems remained compact throughout the simulation. The MT showed small but reproducible shifts in Rg compared to WT (early part slightly more expanded in MT, later part converging or slightly more compact depending on timeframe). Overall changes are subtle, indicating the mutation does not substantially change global packing. SASA time series (Figure 9(7)) showed small differences between WT and MT. The mutant tends to show slightly different SASA values compared to WT, consistent with local rearrangements that expose or bury small surface patches; but there was no major increase in overall exposed region that would indicate global unfolding.

Projections onto the first two eigen vectors (Figure 9(8) proved that WT and MT populate different regions of conformational space. The MT (red) occupied conformational basins that were shifted relative to WT, and transitions between states occur on different timescales; this implies that the mutation changes the dominant low-frequency motions (collective dynamics) of the protein. The 2D projection of the WT trajectory had the majority of sampling localized to compact clusters exhibiting a relatively restricted conformational landscape. The trajectory occupied a limited subspace and had lesser transitions between distinct states, showing that the wild-type KIF1A motor domain is structurally stable and reserved to a small number of dominant conformational states during the course of the simulation. This implies that the native protein maintains well-defined structural dynamics, probably optimized for efficient ATP

turnover and motor function.

The mutant trajectory explored a much broader conformational space, forming multiple distinct clusters that were more widely separated compared to the WT. The MT also showed frequent transitions between clusters, reflecting enhanced conformational flexibility and heterogeneity. This indicates that the mutation promotes structural rearrangements across the simulation, thereby enabling the mutant protein to access conformations not sampled by the WT. The backbone RMSD analysis showed that while both WT and MT achieved stability, the MT consistently diverged away from the reference structure, indicating increase in structural mobility. Residue-level fluctuations (RMSF) were greater in the MT at specific loop regions and functional motifs, especially those involved in ATP binding and hydrolysis. Hydrogen bond analysis showed that the MT formed lesser intramolecular hydrogen bonds compared to the WT. This implied reduced internal stabilization and contributing to the observed flexibility. Finally, the radius of gyration analysis suggested that both WT and MT retained overall structural compactness, although the MT displayed slightly larger fluctuations, consistent with increased local breathing motions.

The FELs derived from the 100-ns trajectories of wild type (Figure 9) and R350G mutant (Figure 9) show clear differences in the conformational thermodynamics and accessible metastable states of the KIF1A motor domain. In the wild-type, FEL is dominated by a single, deep energy basin located near the start of the PC1–PC2 plane, with one or two minor subsidiary wells. This topology implies a strongly preferred conformational substate with relatively large energy barriers separating it from other regions of phase space. This is consistent with a structurally stable motor domain sampling a narrow ensemble of functionally optimized conformations.

The R350G mutant FEL reveals multiple, spatially separated minima distributed across a broader area of the PC1–PC2 plane. These minima are of comparable depth having many metastable basins rather than one overwhelmingly dominant basin, and the inter-basin ridges are lower and more irregular than in the wild type. The mutant hence samples a wider conformational ensemble with more frequent transitions between substates during the simulation timeframe. Taken together with the earlier PCA, RMSD and RMSF results, the FEL topology for R350G displays reduced energetic confinement and an increased population of alternative, accessible conformations.

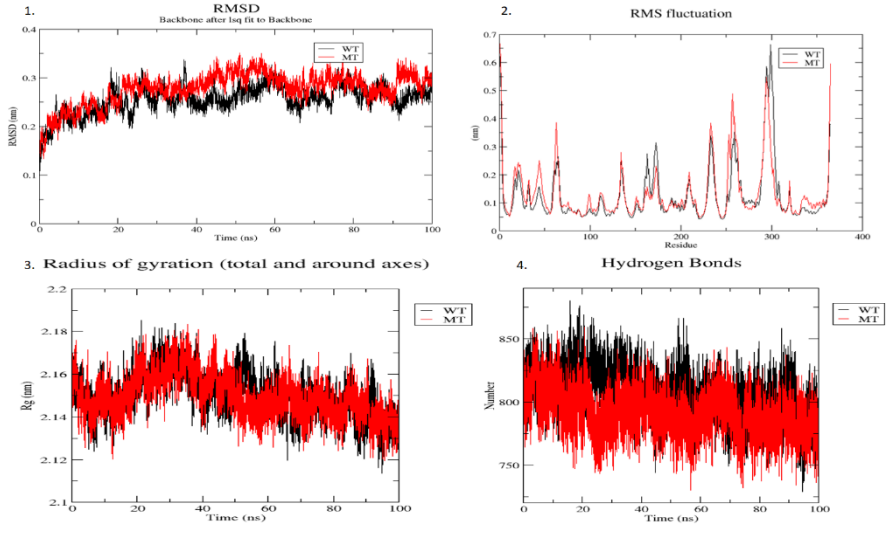

Figure 8: ***1.*** *Backbone RMSD of Wild Type (black) and R350G mutant (red) KIF1A over 100 ns. MT displays a higher mean RMSD and larger fluctuations.* ***2.*** *Per-residue RMSF for WT (black) and R350G mutant (red), showing increased flexibility in several loop regions of the mutant.* ***3.*** *Radius of gyration for WT (black) and MT (red). Small, reproducible differences are present but both remain compact.* ***4.*** *Total hydrogen bonds over time for WT (black) and R350G mutant (red). Mutant exhibits a modest reduction and larger variability in H-bond count.*

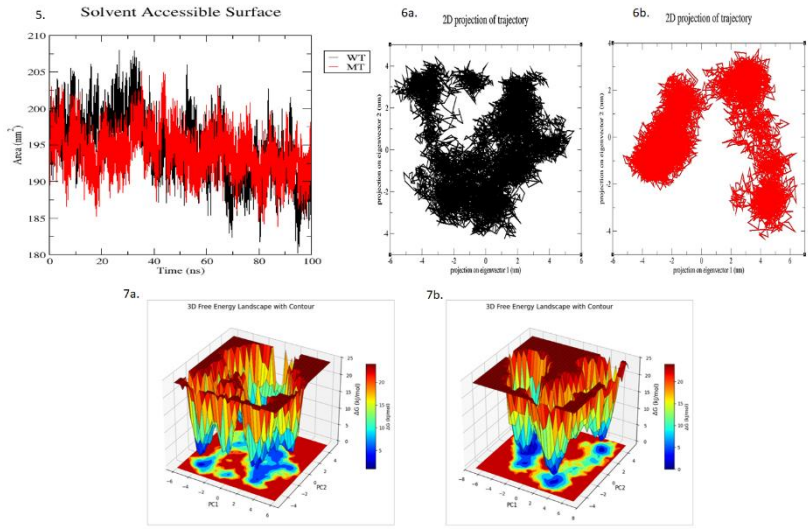

Figure 9: ***5.*** *Solvent accessible surface area of WT (black) and R350G (red) over the trajectory.* ***6.*** *2D Projection of trajectory WT and MT occupy different conformational basins, indicating altered collective motions in the mutant.* ***7.*** *Three-dimensional Free Energy Landscape (FEL) analysis of KIF1A* ***(a)*** *wild-type and* ***(b)*** *R350G. Wild type shows deeper peaks which are more in number as compared to Mutant type.*

DISCUSSION

Deleterious nsSNPs are critical variants that can alter protein structure and function, potentially leading to disease. From the total variants retrieved from dbSNP and ClinVar, 1,198 common nsSNPs were identified. This formed the basis for subsequent analyses, providing a widely accepted dataset. Initial screening using the SIFT tool classified 25 nsSNPs as deleterious, 235 as tolerated, and the remaining 938 were not found in SIFT's database. Deleterious nsSNPs are classified as such because they could potentially alter KIF1A protein function, leading to undesirable changes. The dbNSFP analyses of these 25 nsSNPs by various tools further refined these results, with each tool using its own algorithms and criteria to classify nsSNPs as deleterious or non-deleterious. Align GVGD further classified 5 highly deleterious nsSNPs in the Class 65 category, confirming strong disease association potential. Through multiple tools such as PROVEAN, VEST4, REVEL, and MetaLR, the most deleterious nsSNPs were filtered. SNP&GO, PhD-SNP, and Meta-SNP identified three major mutations, R350G, R1176W, and T99M — as consistently pathogenic, indicating their potential to cause disease. Since these tools base predictions on Gene Ontology, sequence, and evolutionary conservation, these three nsSNPs were selected for further studies [31,32].

Protein stability prediction using MuPro and DUET narrowed the focus to two mutations, R1176W and R350G, which were consistently predicted to decrease stability (negative ΔΔG values) and exert destabilizing effects, particularly in the loop regions of the secondary structure. This reduction indicates conformational changes that could disrupt normal protein function. ConSurf analysis for evolutionary conservation confirmed that these residues are highly conserved (score 9) and located on the exposed regions of the protein, suggesting functional importance. Being highly conserved implies that these residues are crucial for proper KIF1A function, particularly in the motor or cargo-binding domains [33]. Homology modeling and validation revealed that both wild-type and mutant structures retained good overall stereochemical quality, with ERRAT scores above 93, indicating model reliability. RC Plot analysis showed minor changes in the additionally and generously allowed regions, whereas the most favored and disallowed regions remained consistent, indicating localized rather than global structural disruption [34]. Functional impact analysis using MutPred showed that although both mutations scored highly (~9), R350G(rs387907259) exhibited more pronounced functional effects, including alterations in transmembrane protein interactions, DNA binding, disordered interfaces, and gain of methylation. InterPro database search revealed that R350G lies within the Kinesin Motor Domain, a region critical to causing KAND. Hence, R350G was selected as the Mutant Type (MT) for subsequent affinity and stability studies [35].

Docking results indicated that the R350G substitution in KIF1A increases ligand binding, with the mutant displaying a binding affinity of –8.7 kcal/mol compared to –8.5 kcal/mol for the wild type. In kinesins, small conformational changes can significantly affect motor activity, making even minor differences in binding energy functionally meaningful [36]. Literature reports R350G as a hyperactivating mutation, resulting in excessive transport of synaptic vesicle precursors. The observed increase in binding affinity aligns with structural changes that destabilize inhibitory interactions, allowing conformations favoring ligand binding. Replacing the bulky, positively charged arginine with glycine increases local flexibility and reduces electrostatic restrictions, creating a more favorable binding environment. Such gain-of-function alterations may underlie the pathological hyperactivation observed in patients [37].

LigPlot comparisons reveal both conserved and new interactions that enhance ATP affinity in the R350G mutant. The retention of key hydrogen bonds with residues such as Gly100, Ala101, Ser104, Asn200, and Thr213 indicates that the ATP-binding structure of the kinesin motor domain remains intact. Additional stabilizing interactions, particularly with Ser214(A) and Arg203(A), enhance the electrostatic and

hydrogen-bonding environment, while new hydrophobic contacts (Lys110, Met109) improve packing within the binding cleft, compensating for the local flexibility introduced by R350G. These structural changes explain the slightly improved docking score (–8.7 kcal/mol) observed for the mutant [38]. Mechanistically, higher ATP affinity suggests a greater likelihood of productive ATP binding and hydrolysis, processes essential to KIF1A's mechanochemical cycle. Increased nucleotide-binding strength enhances microtubule-based transport efficiency, promoting catalytic turnover by stabilizing ATP binding during the power-stroke phase. Thus, the R350G mutation exhibits an allosteric effect that enhances ATP binding through changes in the hydrogen-bonding and hydrophobic microenvironment, supporting a functional gain in ATP affinity [39].

Molecular dynamics simulations indicated small but consistent changes in the dynamics of R350G. Slightly higher backbone RMSD, local RMSF increases in specific loop regions, a small reduction and greater variation in hydrogen-bond count, and minor shifts in Rg and SASA were observed. Altered sampling of collective motions (PCA) suggests that gain-of-function phenotype of KIF1A, enhancing ATP binding, hydrolysis, and transport activity along microtubules, which may contribute to KAND pathology [41,42]. These findings suggest that the R350G(rs387907259) mutation induces a hyperdynamic state in KIF1A, expanding conformational sampling and increasing flexibility in functionally important regions without compromising the global fold. The consistency across PCA, RMSD, RMSF, hydrogen-bond, and Rg analyses strengthens this conclusion and provides a mechanistic link between the mutation and its gain-of-function phenotype.

CONCLUSION

This study employed a comprehensive silico framework combining multiple computational approaches to identify, characterize, and interpret deleterious nsSNPs within the *KIF1A* gene that causes *KIF1A*-associated neurological disorder (KAND). By systematically screening variants from dbSNP and ClinVar, followed by multi-tier deleteriousness predictions using SIFT, Align-GVGD, Meta-SNP, SNP&GO, PhD-SNP, and REVEL, we successfully narrowed down potential disease-causing variants. Among these, R350G and R1176W were the most deleterious, exhibiting high conservation scores, destabilizing effects on protein R350G perturbs local structural packing and dynamic behavior without causing global destabilization or unfolding over the 100-ns timescale. These changes are consistent with the replacement of arginine with glycine at position 350, which disrupts local stabilizing interactions, increases backbone flexibility, and affects adjacent secondary structures [40]. Although global folding remains intact, these local dynamic changes are functionally relevant if residue 350 is located near regions critical for force generation, microtubule interaction, or allosteric communication. Disruption of local interactions and collective motions may regulate KIF1A's mechanochemical cycle, including ATPase activity, microtubule affinity, and processivity. Comparative PCA analysis showed that the WT protein sampled a narrow conformational subspace, whereas the MT explored a larger phase space, indicative of increased conformational plasticity. Reduced hydrogen bonds support faster structural rearrangements and conformational transitions. Rg analysis confirmed the global fold is preserved, suggesting the mutation fine-tunes local flexibility rather than destabilizing overall structure. These alterations align with the reported structure, and strong associations with functional impairment. Structural and dynamic analyses revealed that the R350G mutation induced local destabilization while preserving global fold integrity, implying an altered dynamic equilibrium and not complete denaturation. Molecular docking and dynamics simulations showed that this mutation increases ATP-binding affinity, alters the hydrogen bond network, and increases conformational flexibility indicating a hyperactive motor state. These gain-of-function traits are related to the phenotypes in KAND. This combination of sequence-based predictions with structural and dynamic analyses highlights the importance of a multi-parametric computational pipeline in understanding the molecular mechanisms underlying neurological disorders. This work lays a foundation for both experimental and therapeutic exploration. Functional validation through *in vitro* assays can substantiate the predicted hyperactivity of mutant *KIF1A*. Also integrating cryo-EM or NMR structural data could further clarify dynamic interpretations. The identified residues may serve as potential targets for small molecules or allosteric modulators that aim in restoring motor regulation. Machine learning models trained on multi-omic data could enhance predictive precision for novel variants, enabling earlier diagnosis and genotype-based stratification in KAND patients.

ABBREVIATIONS

ALIGN GVGD	Align Grantham Variation and Grantham Deviation
AMPA	α-amino-3-hydroxy-5-methyl-4-isoxazolepropionic acid
ATP	Adenosine TriPhosphate
CHARMM27	Chemistry at HARvard Macromolecular Mechanics
ConSurf	Conservation Surface-Mapping
dbSNP	Database of a Single Nucleotide Polymorphism
DENN/MADD	Differentially Expressed in Normal and Neoplastic cells / MAP-kinase Activating Death Domain protein
FASTA	Fast-All
FEL	Free Energy Landscape
GIT1	G Protein Coupled

	Receptor Kinase Interacting Protein
GMQE	Global Model Quality Estimation
GROMACS	Groningen Machine for Chemical Simulations
GRIP	Glutamate Receptor Interacting Protein
GTP	Guanosine Triphosphate
GTPase	Guanosine Triphosphatase
H bonds	Hydrogen Bonds
HSP	Heat Shock Protein
ID	Intellectual Disability
K1FIA	Kinesin Family Member 1A
KAND	K1FIA Associated Disorder
MetaLR	Meta Logistic Regression
MDS	Molecular Dynamics Simulation
MT	Mutant Type
MuPro	Mutation Protein Stability Prediction Tool
nsSNP	Non-Synonymous Single Nucleotide Polymorphism
PCA	Principal Component Analysis
PDB	Protein Data Bank
Phd SNP	Prediction of Human Deleterious Single Nucleotide Polymorphism
PROVEAN	Protein Variation Effect Analyser
RAB3A	Ras-Associated Protein Rab-3A
REVEL	Rare Exome Variant Ensemble Learner
Rg	Radius of Gyration
RMSD	Root Mean Square Deviation
RMSF	Root Mean Square Fluctuation
rsID	Reference SNP Cluster Identification
SASA	Solvent Accessible Surface Area
SIFT	Sorting Intolerant From Tolerant
SNP	Single Nucleotide Polymorphism
SNP & GO	Single Nucleotide Polymorphism and Gene Ontology
SPC	Simple Point Charge
SVP	Split-Valence Polarized
TRKA	Tropomyosin Receptor Kinase A
Vest4	Variant Effect Scoring Tool 4.0
WT	Wild Type

DECLARATIONS

Acknowledgements

The authors sincerely thank BioNome (https://bionome.in/) for providing the essential resources and support that significantly contributed to the successful completion of this research.

Conflict of Interest

The authors declare no conflict of interest

Funding

This research did not receive any specific grant from funding agencies in the public, commercial, or not-for-profit sectors.

Ethical approval

Not applicable

Informed consent

Not applicable

Authors Contribution

All the authors have equally contributed to this manuscript.

REFERENCES

1. Lu X, Li G, Liu S, Wang H, Zhang Z, Chen B. Bioinformatics Analysis of KIF1A expression and gene regulation network in ovarian carcinoma. International Journal of General Medicine. 2021 Jul 1; Volume 14:3707-17. https://doi.org/10.2147/ijgm.s323591
2. Chiba K, Kita T, Anazawa Y, Niwa S. Insight into the regulation of axonal transport from the study of KIF1A-associated neurological disorder. Journal of Cell Science. 2023 Jan 19;136(5). https://doi.org/10.1242/jcs.260742
3. Montenegro-Garreaud X, Hansen AW, Khayat MM, Chander V, Grochowski CM, Jiang Y, et al. Phenotypic expansion in KIF1A -related dominant disorders: A description of novel variants and review of published cases. Human Mutation. 2020 Sep 21;41(12):2094–104. https://doi.org/10.1002/humu.24118
4. Kumari D, Ray K. Phosphoregulation of kinesins involved in Long-Range Intracellular transport. Frontiers in Cell and Developmental Biology. 2022 Jun 3;10. https://doi.org/10.3389/fcell.2022.873164
5. Liu S, Chen J, Shi L, Deng Y, Wang Z. Research progress of kinesin family in neurological diseases.

Frontiers in cellular Neuroscience. 2009;19. https://doi.org/10.3389/fncel.2025.1527305
6. Hirokawa N, Noda Y, Tanaka Y, Niwa S. Kinesin superfamily motor proteins and intracellular transport. Nature Reviews Molecular Cell Biology. 2009;10(10):62-96. https://doi.org/10.1038/nrm2774
7. Citterio A, Arnoldi A, Panzeri E, Merlini L, D'Angelo MG, Musumeci O, et al. Variants in KIF1A gene in dominant and sporadic forms of hereditary spastic paraparesis. Journal of Neurology. 2 018.
8. Ramensky V. Human non-synonymous SNPs: server and survey. Nucleic Acids Research. 2002 Aug 30;30(17):3894-900. https://doi.org/10.1093/nar/gkf493
9. Zhao N, Han JG, Shyu CR, Korkin D. Determining Effects of Non-synonymous SNPs on Protein-Protein Interactions using Supervised and Semi-supervised Learning. PLoS Computational Biology. 204 May 1;10(5):e1003592. https://doi.org/10.1371/journal.pcbi.1003592
10. Dakal TC, Kala D, Dhiman G, Yadav V, Krokhotin A, Dokholyan NV. Predicting the functional consequences of non-synonymous single nucleotide polymorphisms in IL gene. Scientific Reports. 2017 Jul 20;7(1). https://doi.org/10.1038/s41598-017-06575-4
11. Rodriguez-Casado A. In silico investigation of functional nsSNPs- an approach to rational drug design. Research and Reports in Medicinal Chemistry. 2012 Nov 1;31. https://doi.org/10.2147/rrmc.s28211
12. Leelabati Biswas; Protein modeling and in silico analysis to evaluate the pathogenicity of genetic variants in patients with KIF1A-associated neurologic disorder (KAND) ocular phenotypes.. Investigative Ophthalmology Visual Science. 2025;66(8):1844.
13. Kumar R, Madhavan T, Ponnusamy K, Sohn H, Haider S. Computational study of the motor neuron protein KIF5A to identify nsSNPs, bioactive compounds, and its key regulators. Frontiers in Genetics. 2023 Nov 10;14. https://doi.org/10.3389/fgene.2023.1282234
14. Mizuhara Y, Takano M. Biased Brownian Motion of KIF1A and the Role of Tubulin's C-Terminal Tail Studied by Molecular Dynamics Simulation. International Journal of Molecular Sciences. 2021 Feb 4;22(4):1547. https://doi.org/10.3390/ijms22041547
15. Sherry ST. dbSNP: the NCBI database of genetic variation. Nucleic Acids Research. 2001 Jan 1;29(1):308–11. https://doi.org/10.1093/nar/29.1.308
16. Landrum MJ, Chitipiralla S, Kaur K, Brown G, Chen C, Hart J, et al. ClinVar: updates to support classifications of both germline and somatic variants. Nucleic Acids Research. 2024 Nov 23;53(D1):D1313–21. https://doi.org/10.1093/nar/gkae1090
17. Poon KS. In silico analysis of BRCA1 and BRCA2 missense variants and the relevance in molecular genetic testing. Scientific Reports. 2021 May 27;11(1). https://doi.org/10.1038/s41598-021-88586-w
18. Yang CH, Lin GC, Wu CH, Chen JB, Chuang LY. Prediction tools for assessing functional impacts of gene mutations in Clear Cell Renal Cell Carcinoma: A comparative study. Computers in Biology and Medicine. 2025 Apr 29;192:110187. https://doi.org/10.1016/j.compbiomed.2025.110187
19. Andhika NS, Biswas S, Hardcastle C, Green DJ, Ramsden SC, Birney E, et al. Using computational approaches to enhance the interpretation of missense variants in the PAX6 gene. European Journal of Human Genetics. 2024 Jun 7;32(8):1005–13. https://doi.org/10.1038/s41431-024-01638-3
20. Chen J, Li Z, Wu Y, Li X, Chen Z, Chen P, et al. Identification of pathogenic missense mutations of NF1 using computational approaches. Journal of Molecular Neuroscience. 2024 Oct 7;74(4). https://doi.org/10.1007/s12031-024-02271-x
21. Capriotti E, Fariselli P. PhD-SNPg: a webserver and lightweight tool for scoring single nucleotide variants. Nucleic Acids Research. 2017 Apr 24;45(W1):W247–52. https://doi.org/10.1093/nar/gkx369
22. Biswas S, Bagchi A. Mutational impact on "in-Between-Ring" (IBR) domain of PARKIN on protein stability and function. Applied Biochemistry and Biotechnology. 2021 Jan 20;193(6):1603–16. https://doi.org/10.1007/s12010-021-03491-2
23. Seifi M, Walter MA. Accurate prediction of functional, structural, and stability changes in PITX2 mutations using in silico bioinformatics algorithms. PLoS ONE. 2018 Apr 17;13(4):e0195971. https://doi.org/10.1371/journal.pone.0195971
24. Darapaneni V. Large-scale analysis of SARS-CoV-2 envelope protein sequences reveals universally conserved residues. Microbes and Infectious Diseases. 2022; 3(4): 780-783.
25. Bienert S, Waterhouse A, De Beer T a. P, Tauriello G, Studer G, Bordoli L, et al. The SWISS-MODEL Repository—new features and functionality. Nucleic Acids Research. 2016 Nov 29;45(D1):D313–9. https://doi.org/10.1093/nar/gkw1132
26. Hollingsworth SA, Karplus PA. A fresh look at the Ramachandran plot and the occurrence of standard structures in proteins. BioMolecular Concepts. 2010 Sep 8;1(3–4):271–83. https://doi.org/10.1515/bmc.2010.022
27. Wanarase SR, Chavan SV, Sharma S, D S. Evaluation of SNPs from human IGFBP6 associated with gene expression: an in-silico study. Journal of Biomolecular Structure and Dynamics. 2023 Mar 22;41(23):13937–49. https://doi.org/10.1080/07391102.2023.2192793
28. Ridha F, Gromiha MM. MPA-MutPred: a novel strategy for accurately predicting the binding affinity change upon mutation in membrane protein complexes. Briefings in Bioinformatics. 2024 Sep 23;25(6). https://doi.org/10.1093/bib/bbae598
29. Paggi JM, Pandit A, Dror RO. The art and science of molecular docking. Annual Review of Biochemistry. 2024 Apr 10;93(1):389–410. https://doi.org/10.1146/annurev-biochem-030222-120000
30. Redhwan A, Adnan M, Bakhsh HR, Alshammari N, Surti M, Parashar M, et al. Computational identification and functional analysis of potentially pathogenic NSSNPs in

the NLRP3 gene linked to Alzheimer's disease. Cell Biochemistry and Biophysics. 2024 Aug 21; https://doi.org/10.1007/s12013-024-01465-9
31. Ng PC, Henikoff S. SIFT: predicting amino acid changes that affect protein function. Nucleic Acids Res. 2003;31(13):3812–3814. https://doi.org/10.1093/nar/gkg509
32. Liu X, Li C, Mou C, Dong Y, Tu Y, et al. dbNSFP v4: a comprehensive database of transcript-specific functional predictions and annotations for human nonsynonymous and splice-site SNVs. Genome Med. 2020;12:103. https://doi.org/10.1186/s13073-020-00788-6
33. Ashkenazy H, Erez E, Martz E, et al. ConSurf 2016: improved methodology to estimate and visualize evolutionary conservation in macromolecules. Nucleic Acids Res. 2016;44:W344–W350. https://doi.org/10.1093/nar/gkw408
34. Laskowski RA, MacArthur MW, Moss DS, Thornton JM. PROCHECK: a program to check the stereochemical quality of protein structures. J Appl Crystallogr. 1993;26:283–291. https://doi.org/10.1107/S0021889892009944
35. Jones DT, Cozzetto D. DISOPRED3: precise disordered region prediction with annotation for functional residues. Bioinformatics. 2015;31:857–863. https://doi.org/10.1093/bioinformatics/btu744
36. Trott O, Olson AJ. AutoDock Vina: improving the speed and accuracy of docking with a new scoring function, efficient optimization, and multithreading. J Comput Chem. 2010;31:455–461. https://doi.org/10.1002/jcc.21334
37. Chiba K, Shimizu K, Abe M, et al. Gain-of-function mutations in KIF1A hyperactivate axonal transport. Nat Commun. 2019;10:1213. https://doi.org/10.1038/s41467-019-09105-5
38. Wallace AC, Laskowski RA, Thornton JM. LIGPLOT: a program to generate schematic diagrams of protein–ligand interactions. Protein Eng. 1995;8:127–134. https://doi.org/10.1093/protein/8.2.127
39. Morris GM, Huey R, Lindstrom W, et al. AutoDock4 and AutoDockTools4: automated docking with selective receptor flexibility. J Comput Chem. 2009;30:2785–2791. https://doi.org/10.1002/jcc.21256
40. Abraham MJ, Murtola T, Schulz R, et al. GROMACS: High performance molecular simulations through multi-level parallelism from laptops to supercomputers. SoftwareX. 2015;1–2:19–25. https://doi.org/10.1016/j.softx.2015.06.001
41. Amadei A, Linssen AB, Berendsen HJ. Essential dynamics of proteins. Proteins. 1993;17:412–425. https://doi.org/10.1002/prot.340170408
42. Komeili A, Vali H, Beveridge TJ, Newman DK. Molecular dynamics simulations in protein functional analysis: understanding structural flexibility and function. Biophys J. 2010;99:342–350. https://doi.org/10.1016/j.bpj.2010.04.012